Journal of Power Sources 196 (2011) 2475–2482

Contents lists available at ScienceDirect

Journal of Power Sources

journal homepage: www.elsevier.com/locate/jpowsour

Fabrication of anode support for solid oxide fuel cell using zirconium hydroxide as a pore former

Minchul Kim, Jaehyung Lee, Joo-Hwan Han*

School of Materials Science and Engineering, Yeungnam University, Gyeongsan, Gyeongbuk 712-749, Republic of Korea

ARTICLE INFO

Article history:
Received 19 August 2010
Received in revised form 19 August 2010
Accepted 29 October 2010
Available online 18 November 2010

Keywords:
Solid oxide fuel cell
Anode
Pore former
Electrolyte
Zirconium hydroxide

ABSTRACT

A novel method of fabricating NiO–YSZ (yttria stabilized zirconia) anode substrates is developed using a composite pore former, i.e., PMMA (polymethyl-methacrylate) and carbon black or zirconium hydroxide $Zr(OH)_4$. By utilizing a composite pore former, both the shrinkage and porosity, which must be compatible with that of the electrolyte film and sufficient for the fuel supply and exhaust, are easily tailored. Carbon black and the inorganic pore former ($Zr(OH)_4$) affect the shrinkage of the anode substrate more effectively than its porosity, while the polymer spheres (PMMA) adjust the porosity more effectively. In particular, the successful use of zirconium hydroxide as a fine pore former, instead of carbon black, suggests that other zirconium or nickel compound derivatives may be used as pore formers.

1. Introduction

Solid oxide fuel cells (SOFCs) have received a great deal of attention as promising systems for electrical power generation because of their high power conversion efficiency and pollution-free operation [1–4]. In particular, SOFCs based on anode-supported electrolyte films have been under active research in the past few decades due to their excellent performance, especially at intermediate temperatures [1,2]. Nickel oxide–yttria stabilized zirconia (NiO–YSZ) composite is the material used most frequently as the anode in solid oxide fuel cells due to its high electrochemical activity for the oxidation of hydrogen, high electrical conductivity, high thermodynamic stability, and compatibility with the other components of the cell [1,5,6].

To maximize the oxidation reaction and the resultant cell performance, the anode used as the substrate for the electrolyte film should have sufficient porosity to supply the fuel and remove the reaction products. The pore channel network developed by the connected pores provides pathways for transporting the fuel to the sites of the triple-phase boundary and transporting the fuel oxidation products and water vapour away from these sites. During operation of the SOFC, concentration polarization can be avoided by the fast diffusion of the fuel and the reaction products through the whole anode substrate. The electrical conductivity of the anodes should also be sufficiently high to transport the electrons produced by the oxidation reaction to the external current-collector to prevent electrical polarization. Moreover, high electrochemical activity and good compatibility with the other fuel cell components, especially the matching of its sintering shrinkage with that of the electrolyte, are necessary to produce high-quality anodes for SOFCs [7–12].

Many methods have been proposed [4,8,13–15] to provide an anode substrate with suitable porosity for gas diffusion. The most effective and popular method of forming a porous microstructure is the addition of pore formers to the NiO–YSZ composite powders [9]. Flour, rice or corn starch, graphite and spherical polymers are widely used as pore formers [9,11,16]. Thus, the microstructure and pore structure are also significantly influenced by the size, shape and quantity of the pore formers [17,18]. In fact, not only the porosity but also the sintering shrinkage is of great importance in the successful fabrication of anode-supported electrolyte film cells, and, therefore, the sintering shrinkage of the anode should be close to that of the electrolyte film to decrease the stress between them upon sintering. The immoderate stress caused by shrinking mismatch may produce cracks in the electrolyte film, distort the fuel cell and, in turn, diminish the cell performance [10].

Zirconium hydroxide $Zr(OH)_4$, is used in this work as a new pore former together with poly(methyl methacrylate) (PMMA) and carbon black powders. The anode substrate and anode functional layer prepared with the proposed pore former have the potential to provide appropriate porosity as well as suitable shrinkage that matches well with that of the YSZ electrolyte film.

* Corresponding author. Tel.: +82 53 810 2567; fax: +82 53 810 4628.
E-mail address: jhhan@yu.ac.kr (J.-H. Han).

0378-7753/$ – see front matter © 2010 Elsevier B.V. All rights reserved.
doi:10.1016/j.jpowsour.2010.10.109

2. Experimental

Commercially available YSZ containing 8 mol.% Y_2O_3 (TZ-8YS, Tosho Co., Shunan, Japan) and NiO (NiO-FP, Sumitomo Metal Mining Co., Ltd., Tokyo, Japan) powders were used for the fabrication of the NiO–YSZ anode substrate. The average particle sizes of the YSZ and NiO powders as determined by a particle size analyzer (LS 13 320, Porous Material Inc., Brea, CA, USA) were 0.2 and 0.3 μm, respectively. Poly(methyl methacrylate) (PMMA) (LDX-50, Sunjin Chem. Co., Ltd., Ansan, Korea), carbon black (HIBLACK 170, Evonik Carbon Korea, Incheon, Korea) and zirconium hydroxide ($Zr(OH)_4$) (97%, Sigma-Aldrich Co., St. Louis, MO, USA) powders were also used as pore formers. The average particle size of the PMMA spheres was determined to be 5 μm by the manufacturer. The powder mixtures for the anode substrate were prepared according to the compositions indicated in Table 1. Each powder mixture was ball milled in a polyethylene bottle for 6 h with a methyl alcohol medium to which a dispersant (EFKA 4401, Ciba Canada Ltd., Mississauga, Canada) was added. The slurry of powder mixtures was dried at 50 °C overnight and then ground in an agate mortar to form powders for pressing.

These powders were pressed into discs of 20 mm diameter at a pressure of 30 MPa. The powder compacts then were pre-sintered at 1100 °C for 1 h to obtain sufficient mechanical strength for handling. The compacts were heated to the pre-sintering temperature at a rate of 2 °C min^{-1} up to 600 °C and at 5 °C min^{-1} from 600 to 1100 °C, then held for 1 h at 160 °C, 3 h at 350 °C and 1 h at 600 °C for the complete burn-out of the organic additive and PMMA. After measuring the dimensions and weights, the pre-sintered compacts, were sintered by heating at 5 °C min^{-1} to 1400 °C and then held at this temperature for 3 h. The dimensions and weights of the sintered compacts were also measured before heat treatment at 900 °C for 3 h in argon containing 5 vol.% hydrogen for the purpose of reducing the NiO in the sintered compacts to Ni. Then the dimensions and weights of the reduced discs were measured again. These measurements were conducted to determine the linear shrinkage that occurred during each heat-treatment process and the resultant porosity of the disc.

The porosity of the reduced discs (anode substrates) was measured by the Archimedes method. The gas permeability of the reduced anodes was determined using a capillary flowmeter (CFP-1500 AEL, Porous Material Inc., Ithaca, NY, USA), and the electrical conductivity was measured by the 4-point probe method (CMT-SR1000N, Chang Min Co., Ltd., Sungnam, Korea) using a d.c. power supply (UP-3005D, Unicorn Tech Co., Ltd., Anyang, Korea) and a digital multimeter (Model 2000 6-1/2-Digit DMM, Keithley Instruments Inc., Cleveland, OH, USA). The mechanical strength of the anodes was determined by a bi-axial method (ISO6872:2008E, AG 500E, Shimadzu Co., Kyoto, Japan), and their microstructures were examined with a scanning electron microscope (SEM, S-4200, Hitachi High-technologies Co., Ltd., Tokyo, Japan).

The anode functional layer and YSZ electrolyte films were deposited on the pre-sintered anode substrates by the slurry dip-coating technique [19] and co-sintered at 1400 °C for 3 h in air. The detailed procedures used for fabricating the functional layer and the electrolyte film on the anode substrate are described below in Section 3. To investigate the interfacial polarization resistance of the prepared anode substrate and anode functional layer, a.c. impedance measurements were performed with an impedance analyzer (1260A Impedance/Gain-Phase Analyzer, AMETEK Solartron, Farnborough, United Kingdom) in a wet hydrogen (3 vol.% H_2O–97 or 5 vol.% H_2–balance Ar) atmosphere at 800 °C over the frequency range of 0.1 to 10^5 Hz with an excitation voltage of 50 mV to ensure a linear response.

3. Results and discussion

The porosity of the anode substrate in fuel cells affects their performance and, considering this reason alone, should be as high as possible. The mechanical strength and electrical conductivity of the substrate should also be considered in the fabrication of fuel cells and their performance. These factors decrease with increasing porosity, and hence usually a porosity of around 40 vol.% is regarded as appropriate [20]. On the other hand, matching of the sintering shrinkage between the anode substrate and electrolyte film is very important for the formation of an electrolyte film on the anode substrate [2]. Given the sintering shrinkage of YSZ, which was determined to be 22% in this study, the shrinkage of the anode substrate should be controlled to be close to this value. To determine the sintering shrinkage of YSZ, the YSZ powder used for YSZ film formation was compacted into discs and then cold iso-statically pressed at 135 MPa and sintered at 1400 °C for 3 h.

The variation of the porosity after the reduction treatment and sintering shrinkage of the anode substrate with the amount of pore former added to the powder mixture (56 wt.% NiO–44 wt.% YSZ) is presented in Fig. 1. The first character in the upper abscissa denotes the type of pore former that was used (e.g., P = PMMA, C = carbon black, Z = zirconium hydroxide), and the following digits are the amount of pore former that was added (e.g., P10_Z5 denotes that 10 parts of PMMA and 5 parts of zirconium hydroxide were added to 100 parts of the NiO–YSZ powder mixture, by weight). As expected, the porosity increases with increasing amount of pore former (PMMA). The sintering shrinkage, however, does not vary significantly with the amount of PMMA added, but remains at around 22%, which is close to the sintering shrinkage of the anode substrate without PMMA. Such a negligible variation in the sintering shrinkage, in spite of the increasing amount of PMMA added, reflects the fact that the large pores that develop at the sites of the PMMA spheres are stable and consequently survive (in other words, do not shrink) throughout the whole sintering process. Consequently, no additional sintering shrinkage due to the addition of PMMA is observed. When the amount of PMMA added is 9 wt.% (P10), the porosity and sintering shrinkage reach 40.9 vol.% and 20.7%, respectively.

The appreciable decrease in the sintering shrinkage observed for P10 in Fig. 1 can be explained as follows. The pores from the PMMA spheres, which must be individually isolated at a small level of PMMA addition, are likely to start contacting each other at a critical concentration with increasing PMMA addition, and their contiguity or contact frequency may substantially increase to form

Table 1
Compositions of powder mixtures used for anode substrate and anode functional layer.

Symbol	Methanol (g)	EFKA 4401 (g)	NiO (g)	8YSZ (g)	PMMA (g)	Carbon Black (g)	$Zr(OH)_4$ (g)
Compositions of powder mixtures used for anode substrate							
P0	40	1	56	44	0		
P2, P6, P8, P10	40	1	56	44	2, 6, 8, 10		
P10_C5	40	1	56	44	10	5	
P10_Z5	40	1	56	44	10		5
Composition of powder mixture used for anode functional layer							
Z4.4	40	1	56	39.6			4.4

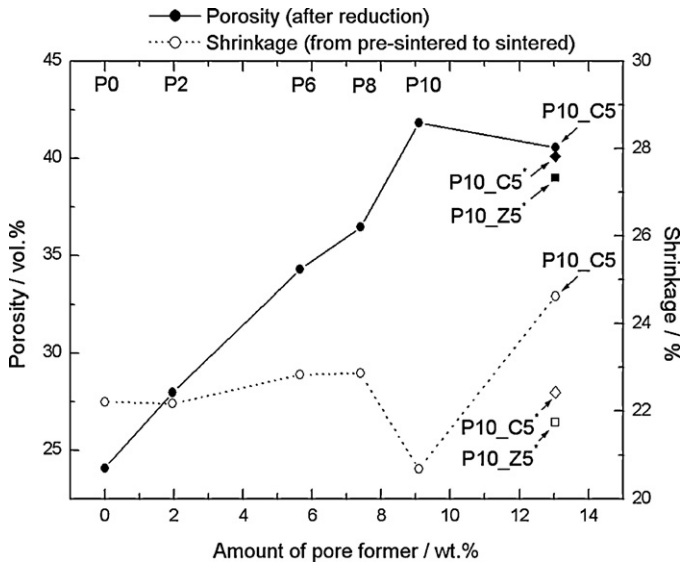

Fig. 1. Variation of porosity and sintering shrinkage of anode substrate with amount of pore former added to powder mixture (56 wt.%NiO–44 wt.%YSZ). The superscripts of P10_C5* and P10_Z5* denote anode substrates being pre-sintered at 1150 °C.

inter-connected pore structures with PMMA addition beyond this concentration. This microstructural change from an isolated to an inter-connected pore structure appears to occur between P8 and P10. Taking the specific gravity of PMMA (1.18 g cm^{-3}) and the theoretical density of the sintered 56 wt.% NiO–44 wt.% YSZ composite (6.33 g cm^{-3}) into account, 30 and 35 vol.% of the anode substrate are estimated to be occupied by PMMA spheres before sintering for P8 and P10, respectively. In Fig. 1, note that the reduction in shrinkage observed for the P10 anode substrate is simultaneously accompanied by a steeper increase in porosity. This observation strongly implies that the shrinkage reduction observed for P10 is closely related to the variation in sintering behaviour due to its microstructural change, and the inter-connected pores retard densification.

The microstructure of the anode substrate fabricated by adding up to 9 wt.% of the PMMA spheres is given in Fig. 2(a) and (b). Spherical pores with a diameter of about 5 μm are homogeneously distributed throughout the anode substrate and are connected to each other to form a pore network channel. The microstructure between the pores is rather dense, however, as can be seen in the micrographs, and is considered not to be beneficial for gas phase transport. To improve the microstructure by creating micropores between the pores, carbon black was also added to the 9 wt.% PMMA-added anode substrate (P10). The effect of adding carbon black on the porosity and shrinkage is found to be the opposite of that induced by the addition of PMMA. A negligible variation in porosity, but an appreciable increase in shrinkage, is observed for the anode substrates to which up to 4 wt.% of carbon black is added (compare P10 and P10_C5 in Fig. 1). This result indicates that the micropores developed at the sites of the carbon black are rather unstable during sintering because of their fine size, and thus a significant amount of them disappear to cause a substantial increase in the shrinkage, but negligible variation in porosity. As shown in Fig. 2(c) and (d), the microstructure between the large pores in the anode substrate to which carbon black is added is more porous than that of the anode substrate without carbon black (Fig. 2(a) and (b)). Moreover, the large pores arising from the PMMA spheres in the carbon black-added anode shrink appreciably during sintering, and the average size of the pores becomes slightly smaller, which is why the porosity of the anode substrate with carbon black is somewhat lower than that of the anode substrate without carbon black, even though an additional pore former (carbon black) is added.

On the other hand, the sintering shrinkage of the anode substrate must be close to that of the electrolyte film (22%), as mentioned above. Thus, it is necessary that the higher sintering shrinkage of the P10_C5 anode substrate (24.6%) be lowered by increasing the pre-sintering temperature. With the increased pre-sintering shrinkage obtained by increasing the pre-sintering temperature from 1100 to 1150 °C, the sintering shrinkage of the P10_C5* anode substrate can be reduced to 22.4% without changing its porosity, as shown in Fig. 1. The superscripts of P10_C5* and P10_Z5* denote that the anode substrates were pre-sintered at 1150 °C. The porosity (40.1 vol.%), sintering shrinkage (22.4%) and resultant microstructure of this anode substrate material are considered to satisfy the abovementioned requirements for high performance anode materials.

Because of its hydrophobic surface characteristics and high specific surface area, the dispersion of carbon black is difficult to achieve, especially in an aqueous system. Carbon black particles are normally agglomerates that are made up of many aggregates that consist of a few nanometer-sized primary particles bonded together [21]. As a consequence of this structure, the carbon black particles are extremely porous and, therefore, have an extremely large surface area. These surface characteristics of carbon black particles, which are quite different from those of oxide particles, prevent stability of the slurry mixture of carbon black and oxide powders. In particular, it is very difficult to attain a high solid loading, due to the high water absorption and nanometer size of the carbon black particles that exist in the slurry mixture.

Thus, a new pore former, zirconium hydroxide $Zr(OH)_4$, as a substitute for carbon black, was used in this work. The advantages of this pore former include the fact that its surface characteristics are likely to be similar to those of the oxide powders employed for the anode substrate materials, and that the particles are nonporous and their sizes are much greater than those of carbon black particles. Furthermore, this pore former additive is based on the same element as one of the ingredients constituting the anode substrate material, Zr, and transforms to zirconia during sintering. This concept for choosing the pore former could be extended to the use of other zirconium and/or nickel compound derivatives, such as zirconium carbonate, nickel hydroxide, and nickel carbonate.

Instead of carbon black, zirconium hydroxide was added to the 9 wt.% PMMA-added anode substrate. The effects of adding zirconium hydroxide on the porosity and shrinkage are found to be similar to those of carbon black (compare P10_C5* and P10_Z5* in Fig. 1). Due to the volumetric change arising from the phase transformation from $Zr(OH)_4$ to ZrO_2 during sintering, micropores develop at the sites of the zirconium hydroxide particles, and these play the same role as carbon black particles. As shown in Fig. 2(e) and (f), the microstructure between the large pores is more porous than that of the anode substrate in which PMMA alone is used as the pore former (Fig. 2(a) and (b)). Moreover, the large pores generated due to the PMMA spheres shrink appreciably during sintering, and their average size becomes slightly smaller, which is exactly the same behaviour as that exhibited by the anode substrate prepared by adding both PMMA and carbon black, P10_C5*. Therefore, the porosity (38.3 vol.%), sintering shrinkage (21.7%), and resultant microstructure of this anode substrate material (P10_Z5*) are considered to satisfy the requirements for high-performance anodes quite well.

The variation of (a) the electrical conductivity at room temperature and (b) the bi-axial strength of the anode substrates with the amount of pore former are presented in Fig. 3. Both the electrical conductivity and bi-axial strength decrease monotonically with an increasing amount of PMMA. This behaviour is attributed to the

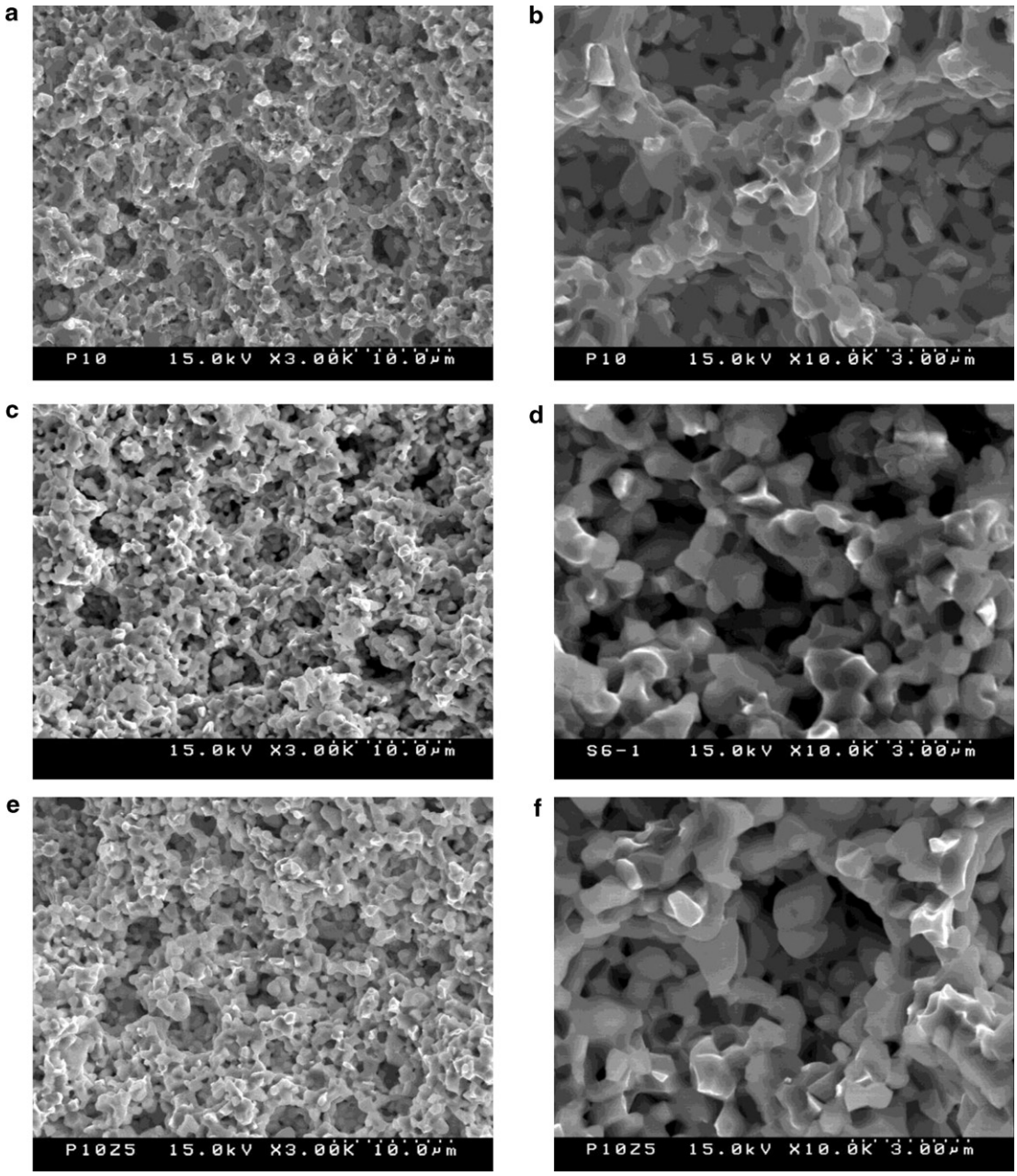

Fig. 2. SEM micrographs showing microstructures of anode substrate fabricated by adding (a) and (b) 9 wt.% PMMA (P10), (c) and (d) 9 wt.% PMMA and 4 wt.% carbon black (P10_C5) and (e) and (f) 9 wt.% PMMA and 4 wt.% $Zr(OH)_4$ (P10_Z5*).

increase in porosity afforded by the addition of PMMA, as noted in Fig. 1. By contrast, the addition of carbon black to the PMMA-added anode materials has a negligible effect on their electrical conductivity and strength, as observed in Fig. 3. Note that such addition does not cause any appreciable variation of porosity, as discussed above, which is why the electrical conductivity and the mechanical strength are relatively insensitive to the addition of the carbon black. These two parameters show similar behaviour in the case of an anode substrate to which zirconium hydroxide is added. The electrical conductivity and mechanical strength of the $Zr(OH)_4$-added anode substrate (P10_Z5*) are 3337 S cm^{-1} and 148 MPa, respectively, which are much higher than those reported for Ni–YSZ composite anode substrates having the same level of porosity [22,23]. Furthermore, the gas permeability is 0.047 cm^2 (cm H_2O)$^{-1}$ min^{-1}, which is higher than the normally reported gas permeability [24].

The PMMA particles used in this work act as templates for forming pores with similar shapes and sizes as a consequence of their burn-out during sintering. The large-size pores formed during sintering at the PMMA particle sites are believed to contribute to the gas phase transport. On the other hand, the micropores in the ceramic structures that are formed between the macropores by the addition of the micropore former (zirconium hydroxide and carbon black) and are also produced during the reduction process would greatly increase the triple-phase boundaries (TPBs), which are crucial for the cell performance [1]. Such a cooperative effect of large and small size pores provided by the addition of the composite pore former (PMMA and $Zr(OH)_4$ or carbon black) is therefore considered to enhance greatly the cell performance.

The anode must have sufficiently high electrical conductivity for electron flow in a reducing environment at its operating temperature. The electrical conductivities of the Ni–YSZ anode substrates

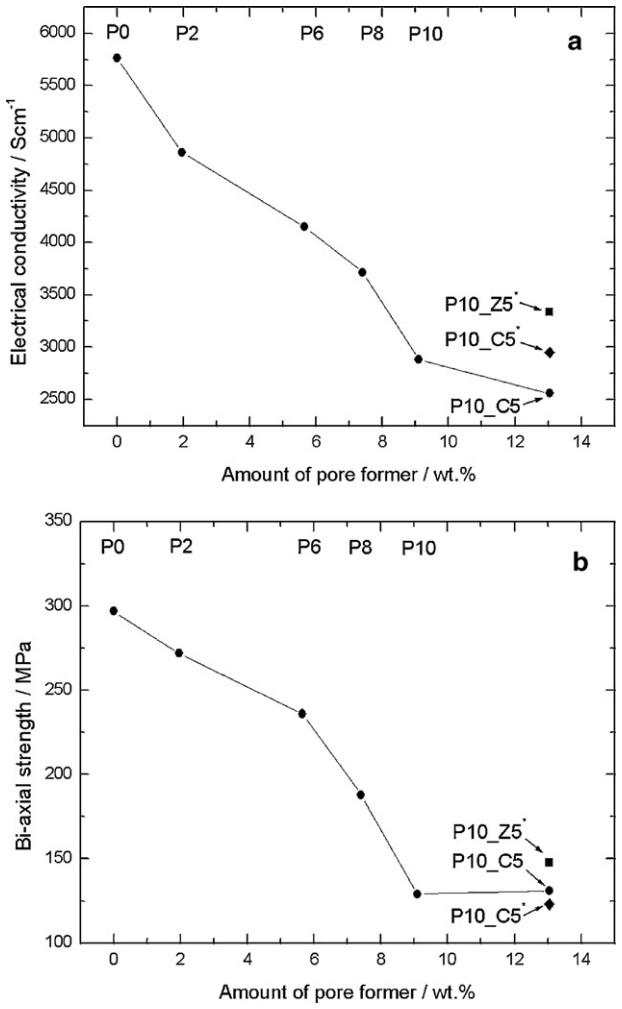

Fig. 3. Variations of (a) electrical conductivity at room temperature and (b) bi-axial strength of anode substrates with amount of pore former. The superscripts of P10_C5* and P10_Z5* denote anode substrates being pre-sintered at 1150 °C.

prepared in this study are plotted as a function of temperature in Fig. 4. The electrical conductivities of more than 10^3 S cm^{-1} at normal operating temperature, e.g., 750 °C, are higher than the literature values measured for anode substrate materials with the same level of porosity [23]. The conduction follows typical metallic behaviour, i.e., the conductivity decreases with increasing temperature, and this indicates that it occurs through the Ni connections. The electrical conductivities of P10, P10_C5*, and P10_Z5* are high enough, and thus they are all applicable for the anode of an SOFC from the standpoint of their electrical conductivity and in terms of their strength and porosity.

On the other hand, lowering the operation temperature of solid oxide fuel cells may allow a significant cost reduction by extending the materials available for constituting SOFC systems [25–27], which can be achieved by reducing the thickness of the electrolyte film layer developed on the anode substrate. The interfacial resistance between the electrolyte and the anode substrate, however, becomes dominant at intermediate temperatures and influences the performance of the cell. Multi-layer anode structures such as those consisting of an anode functional layer formed on the anode substrate have therefore been proposed [25,26,28]. By constructing an anode functional layer with a finer microstructure and making use of the resultant increase of the triple-phase boundary length, activation polarization due to interface resistance can be minimized [25,26,28,29].

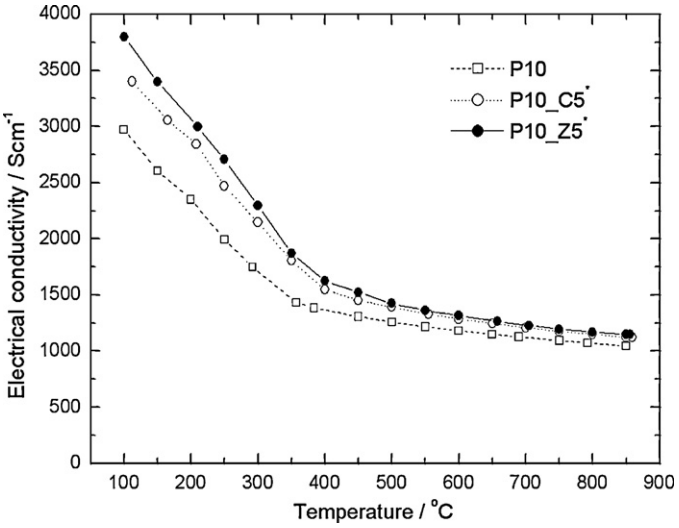

Fig. 4. Electrical conductivities of anode substrates (e.g., P10, P10_C5* and P10_Z5*) plotted as function of temperature.

Fig. 5 shows the variation of porosity (after reduction treatment) and sintering shrinkage of the anode functional layer with the amount of zirconium hydroxide added to the powder mixture with a composition of 56 wt.% NiO–(44–x) wt.% YSZ–x wt.% $Zr(OH)_4$. In the region where small amounts of zirconium hydroxide are added, the porosity increases with increasing amount of zirconium hydroxide. On the other hand, the increase in porosity diminishes with this addition, and the porosity tends to finally saturate. The porosity increase afforded by the addition of zirconium hydroxide can be attributed to the creation of pores due to the phase transformation of $Zr(OH)_4$ to ZrO_2, which occurs during sintering. On the other hand, the sintering shrinkage does not vary significantly with the amount of zirconium hydroxide added but remains around 22%, which is close to the sintering shrinkage of the anode substrate and the electrolyte film. At 4.4 wt.% of $Zr(OH)_4$, the porosity and sintering shrinkage reach 31.8 vol.% and 21.6%, respectively, which are believed to be the most suitable levels for the composition of the functional layer. In particular, the higher electrical conductivity (4045 S cm^{-1}) compared with that of the anode substrate (3337 S cm^{-1} for P10_Z5*) is believed to be beneficial to the fuel cell performance by moderating the activation polarization.

To determine the interfacial polarization resistance of the prepared anode and anode functional layer, a.c. impedance measurements were conducted on Ni–YSZ/YSZ/Ni–YSZ symmetric cells with anode compositions of P10, P10_C5, P10_Z5 and Z4.4. For these measurements, the anode substrate and anode functional layer materials were coated on to both sides of a YSZ electrolyte pellet of 17 mm in diameter and 2.1 mm in thickness, co-fired at 1400 °C for 3 h in air to produce the NiO–YSZ/YSZ/NiO–YSZ cells and then heat-treated at 900 °C for 3 h in 5 vol.% H_2–Ar gas atmosphere for anode reduction. The impedances measured for the symmetric cells at 800 °C in a wet hydrogen atmosphere are given in Fig. 6. The impedance diagram is composed of two clearly separated arcs and this indicates that H_2 oxidation at the Ni–YSZ cermet electrodes is controlled by at least two electrode processes in series. The middle- and high-frequency arcs are, respectively, associated with a slow hydrogen dissociative adsorption or a surface diffusion process at the Ni surface and a charge transfer reaction at the electrode/electrolyte interface [28]. The polarization resistance for a single electrolyte/anode interface is one-half of the difference between the two intercepts with the real axis at high frequencies and low frequencies because the symmetrical cell is composed

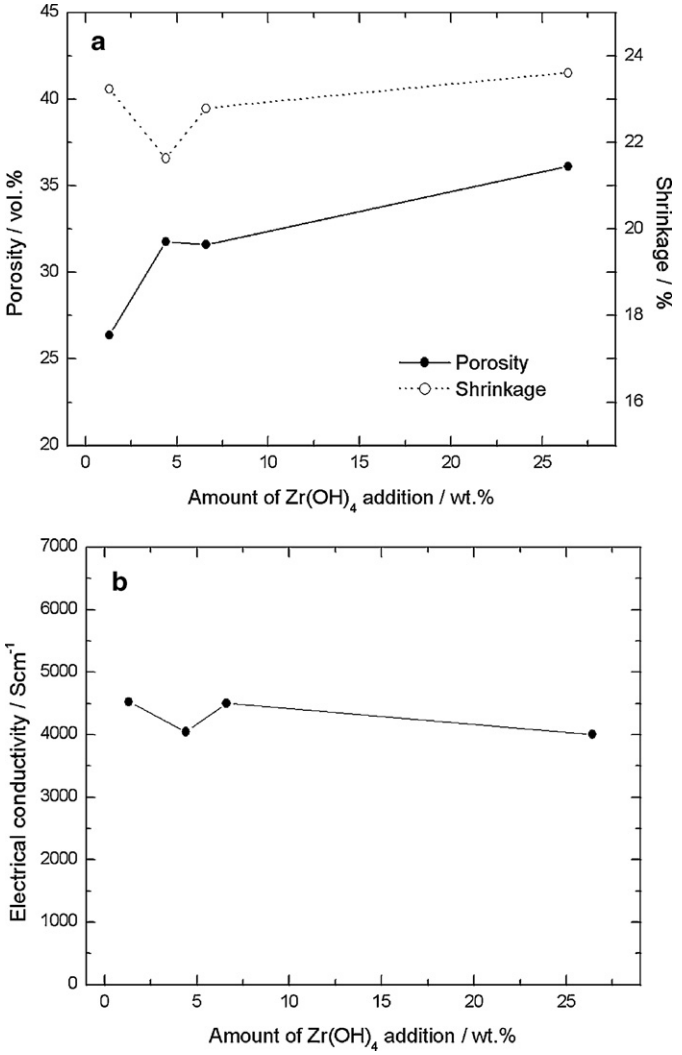

Fig. 5. Variations of (a) porosity (after reduction treatment) and (b) sintering shrinkage of the anode functional layer with amount of zirconium hydroxide added to powder mixture with composition of 56 wt.%NiO–(44−x) wt.%YSZ–x wt.%$Zr(OH)_4$.

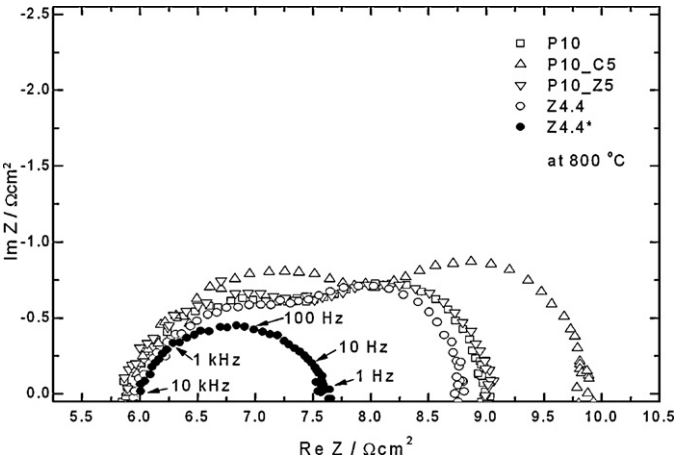

Fig. 6. Impedance curves measured at 800 °C for Ni–YSZ/YSZ/Ni–YSZ symmetric cells with anode composition of P10, P10_C5, P10_Z5 and Z4.4. Numbers indicate frequencies in Hz. Asterisk (*) in Z4.4* denotes its impedance was measured in 97 vol.% H_2–3 vol.% H_2O atmosphere.

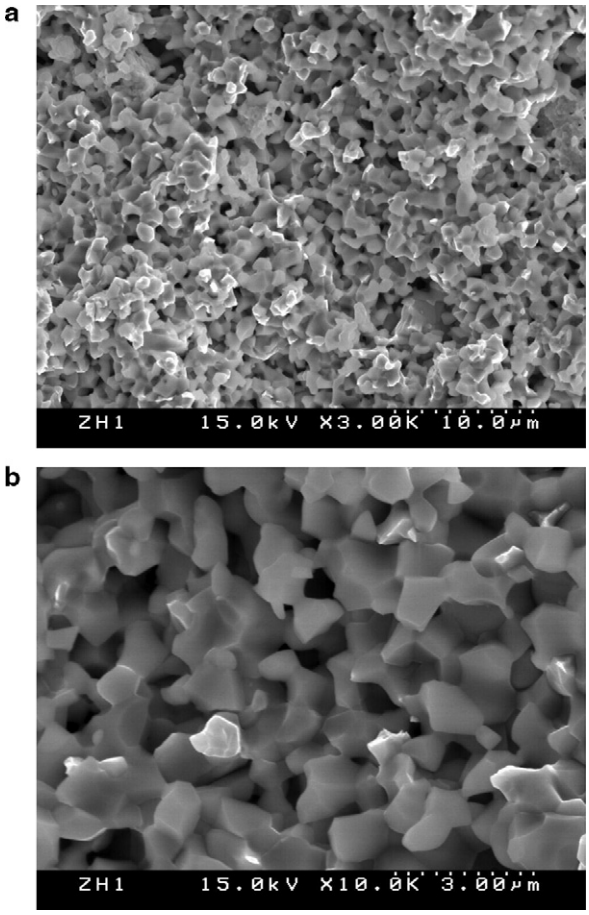

Fig. 7. SEM micrographs of anode functional layer fabricated by adding 4.4 wt.% of $Zr(OH)_4$.

of two Ni–YSZ/YSZ interfaces. As shown in Fig. 6, the interfacial resistance of the anode substrate is improved with the functional layer (Z4.4). In addition, the middle-frequency arc almost disappears when increasing the concentration of hydrogen in the wet atmosphere from 5 to 97%, and thereby indicates that the polarization is mainly caused by the charge transfer reaction in the fuel electrode (anode).

The microstructure of the anode functional layer fabricated by adding up to 4.4 wt.% of zirconium hydroxide is shown in Fig. 7(a) and (b). Pores with a size of about 1 μm are homogeneously distributed throughout the functional layer and are connected to each other to form a pore network channel. Based on the fact that the porosity of the functional layer prepared without adding $Zr(OH)_4$ is determined to be 22.8 vol.% after reduction treatment, the net contribution of the addition of 4.4 wt.% of $Zr(OH)_4$ to the porosity is estimated to be 9.0 vol.%. Note that the porosity of the functional layer prepared with the addition of 4.4 wt.% of $Zr(OH)_4$ after reduction is 31.8 vol.%, as shown in Fig. 5. Such an anode functional layer with a finer microstructure is believed to provide more electrochemically active surfaces (triple-phase boundaries) and thus improves cell performance.

To fabricate the functional layer on the anode substrate presintered at 1150 °C for 1 h, a dip-coating slurry was prepared by the addition of zirconium hydroxide to the NiO–YSZ powder mixture, with a composition of 56.0 wt.% NiO–39.6 wt.% YSZ–4.4 wt.% $Zr(OH)_4$. The powder mixture used for the function layer was ball-milled for 18 h with zirconia balls in a liquid medium that consisted of methyl alcohol containing 1 wt.% of EFKA 4401 as a dispersant. After adding a 3 wt.% of polyvinyl butyral resin binder (Butvar B-98,

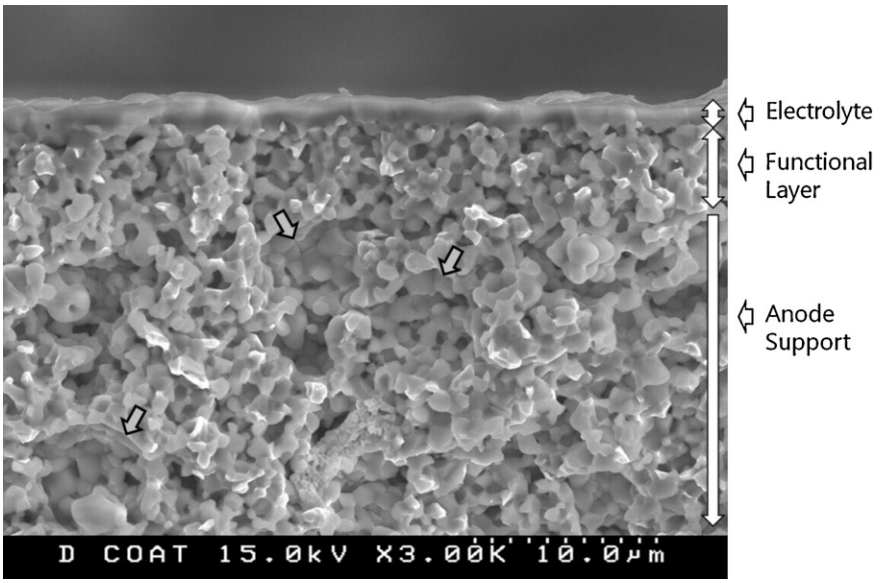

Fig. 8. SEM micrograph of anode functional layer and electrolyte film coated anode substrate.

Solutia Inc., St. Louis, MO, USA) and 2 wt.% of DOP (dioctyl phthalate, 99.0%, Samchun Pure Chem. Co., Ltd., Pyongtack, Korea) plasticizer, the slurry was further ball-milled for 5 h. The solid loading of the dip-coating slurry was then controlled to be 10 wt.%. The functional layer was formed on the pre-sintered anode substrate using a dip-coating machine by holding the substrate in the slurry for 30 s and conducting this coating process twice. The anode substrate, on which the functional layer was coated, was dried at room temperature for 1 h, and then an electrolyte film layer was also formed on the dried functional layer by the same dip-coating process. For this process, the slurry used for the electrolyte film coating was prepared by the same process as that of the slurry used for the functional layer coating. The functional layer-coated anode substrate was dipped twice into the slurry for 30 s using the dip-coating machine and then dried at room temperature for 1 h. The anode substrate on which the functional layer and electrolyte film were coated was sintered at 1400 °C for 3 h. The dip-coating processes employed for forming the thin and uniform green YSZ electrolyte film and the anode functional layer were carried out twice for two purposes, namely (1) to guarantee the strength of the electrolyte and the functional layer and (2) to prevent pin holes from developing on the electrolyte film surface during the drying and sintering process [19].

The cross section of the electrolyte film/anode functional layer/anode substrate structure, which was sintered at 1400 °C for 3 h and reduced at 900 °C by H_2 is shown in Fig. 8. The electrolyte film layer is about 3-μm thick and is fully densified without any defects. The key challenge is still the fabrication of fully-dense YSZ electrolyte thin films on porous anode supports without any defects (e.g., cracks, pinholes, etc.) [19]. The functional layer smooths the surface roughness of the anode substrate, which is rather rough due to the presence of large pores in its interior, and improves the roughness of the surface on which the electrolyte will sit. This improved surface roughness may reduce the possibility of electrolyte film defect formation. Furthermore, the functional layer has a fine and homogeneous pore structure and is tightly bonded with the electrolyte and the substrate.

4. Conclusions

The porosity of the anode substrate to which 9 wt.% PMMA and 4 wt.% zirconium hydroxide pore formers are added together is 38.3 vol.% after reduction treatment. It is expected that the large pores produced by the PMMA facilitate the diffusion of the gas, but that the small pores produced by the zirconium hydroxide promote the increase in the length of the TPB. The sintering shrinkage of the anode substrate is 21.7%, which matches well with that of YSZ (22%). Compared with the anode using PMMA as an individual pore former, the additional shrinkage of the anode substrate fabricated with the composite pore formers is generated by the supplementary addition of zirconium hydroxide or carbon black, which is a desirable result and demonstrates the advantage of the composite pore former. The porosity and shrinkage of the anode can be easily adjusted by controlling the amount of composite pore formers and their relative ratio. Zirconium hydroxide or carbon black plays the role of adjusting the total shrinkage, and PMMA is used to adjust the porosity simultaneously. Zirconium hydroxide as a fine pore former is also successful in creating an appropriate amount (31.8 vol.%) of pores of suitable size (~1 μm) in the anode functional layer fabricated on the anode substrate.

Acknowledgments

This research was financially supported by the Ministry of Knowledge Economy (MKE), Korea Institute for Advancement of Technology (KIAT) and Dae Gyeong Leading Industry Office through the Leading Industry Development for Economic Region.

References

[1] Chunwen Sun, Ulrich Stimming, J. Power Sources 171 (2007) 247–260.
[2] Jinyan Hu, Zhe Lü, Kongfa Chen, Xiqiang Huang, Na Ai, Xiaobo Du, Chengwei Fu, Jiaming Wang, Wenhui Su, J. Membr. Sci. 318 (2008) 445–451.
[3] Takehisa Fukui, Kenji Murata, Satoshi Ohara, Hiroya Abe, Makio Naito, Kiyoshi Nogi, J. Power Sources 125 (2004) 17–21.
[4] Yanhong Yin, Wei Zhu, Changrong Xia, Guangyao Meng, J. Power Sources 132 (2004) 36–41.
[5] W.K. Yoshito, J.R. Matos, V. Ussui, D.R.R. Lazar, J.O.A. Paschoal, J. Therm. Anal. Calorim. 97 (2009) 303–308.
[6] C.M. Dikwal, W. Bujalski, K. Kendall, J. Power Sources 193 (2008) 241–248.
[7] Axel C. Müller, Dirk Herbstritt, Ivers-Tiffée Ellen, Solid State Ionics 152–153 (2002) 537–542.
[8] Hibiki Itoh, Tohru Yamamoto, Masashi Mori, Teruhisa Horita, Natsuko Sakai, Harumi Yokokawa, Masayuki Dokiya, J. Electrochem. Soc. 144 (2) (1997) 641–646.
[9] J.J. Haslam, Ai-Quoc Pham, Brandon W. Chung, Joseph F. DiCarlo, Robert S. Glass, J. Am. Ceram. Soc. 88 (3) (2005) 513–518.
[10] Weitao Bao, Qibing Chang, Guangyao Meng, J. Membr. Sci. 259 (2005) 103–109.

[11] R.M.C. Clemmer, S.F. Corbin, Solid State Ionics 166 (2004) 251–259.
[12] Raymond J. Gorte, Seungdoo Park, John M. Vohs, Conghua Wang, Adv. Mater. 12 (19) (2000) 1465–1469.
[13] Sun Dong Kim, Sang Hoon Hyun, Jooho Moon, Jong-Hee Kim, Rak Hyun Song, J. Power Sources 139 (2005) 67–72.
[14] Sung Pil Yoon, Jonghee Han, Suk Woo Nam, Tae-Hoon Lim, Seong-Ahn Hong, J. Power Sources 136 (2004) 30–36.
[15] P. Duran, J. Tartaj, F. Capel, C. Moure, J. Eur. Ceram. Soc. 23 (2003) 2125–2133.
[16] Kongfa Chen, Zhe Lü, Na Ai, Xiqiang Huang, Yaohui Zhang, Xianshuang Xin, Ruibin Zhu, Wenhui Su, J. Power Sources 160 (2006) 436–438.
[17] A. Sanson, P. Pinasco, E. Roncari, J. Eur. Ceram. Soc. 28 (2008) 1221–1226.
[18] E. Gregorová, Willi Pabst, Ivan Bohačenko, J. Eur. Ceram. Soc. 26 (2006) 1301–1309.
[19] Zhenhua Wang, Kening Sun, Shuiyun Shen, Xiaoliang Zhou, Jinshuo Qiao, Naiqing Zhang, J. Solid State Electrochem. 14 (2010) 637–642.
[20] Wei-Ping Dow, Yu-Piao Wang, Ta-Jen Huang, J. Catal. 160 (1996) 155–170.
[21] M. Sharif Sh, F. Golestani Fard, E. Khatibi, H. Sarpoolaky, J. Taiwan Inst. Chem. Eng. 40 (2009) 524–527.
[22] Jiangrong Kong, Kening Sun, Derui Zhou, Jinshuo Qiao, Jigang Li, Anode-supported IT-SOFC anode prepared by tape casting technique, IEEE IFOST2006, 2006, pp. 186–189.
[23] Kee Sung Lee, Shiwoo Lee, Ji Haeng Yu, Doo Won Seo, Sang Kuk Woo, J. Solid State Electrochem. 11 (2007) 1295–1301.
[24] Jang-Weon Heo, Dong-Suek Lee, Jong-Ho Lee, Jae-Dong Kim, Joo-Sun Kim, Hae Weon Lee, Joo-Ho Moon, J. Kor. Ceram. Soc. 39 (1) (2002) 86–91.
[25] Zhenhua Wang, Naiqing Zhang, Jinshuo Qiao, Kening Sun, Ping Xu, Electrochem. Commun. 11 (2009) 1120–1123.
[26] P. Holtappels, C. Sorof, M.C. Verbraeken, S. Rambert, U. Vogt, Fuel Cells 6 (2) (2006) 113–116.
[27] K. Yamahara, Tal Z. Sholklapper, Craig P. Jacobson, Steven J. Visco, Lutgard C. De Jonghe, Solid State Ionics 176 (2005) 1359–1364.
[28] Jiangrong Kong, Kening Sun, Derui Zhou, Naiqing Zhang, Ju Mu, Jinshuo Qiao, J. Power Sources 166 (2007) 337–342.
[29] Jong-Ho Lee, Hae-Weon Lee, Joo-Won Son, Hue-Sup Song, Hyoung-Chul Kim, Hwa-Young Jung, High performance of anode-supported solid oxide fuel cell, United States Patent Application Publication Pub. No. US2007/0015045 A1, January 18, 2007.